AIAA JOURNAL
Vol. 31, No. 6, June 1993

Investigation of a Contoured Wall Injector for Hypervelocity Mixing Augmentation

Ian A. Waitz*
Massachusetts Institute of Technology, Cambridge, Massachusetts 01239
and
Frank E. Marble† and Edward E. Zukoski‡
California Institute of Technology, Pasadena, California 91125

An experimental and computational investigation of a contoured wall fuel injector is presented. The injector was aimed at enabling shock-enhanced mixing for the supersonic combustion ramjet engines currently envisioned for applications on hypersonic vehicles. Three-dimensional flowfield surveys and temporally resolved, planar Rayleigh scattering measurements are presented for Mach 1.7 helium injection into Mach 6 air. These experimental data are compared directly with a three-dimensional Navier-Stokes simulation to provide a detailed characterization of the flow about the injector array. Time-mean mixing rate data and preliminary conclusions concerning various sources for axial vorticity are presented.

Nomenclature

$\bar{A}$ = injectant to freestream area ratio
c_{He} = helium mass fraction
E = hot-film anemometer output
h_i = height of nozzle exit plane
M = Mach number
$\bar{m}$ = injectant to freestream mass flux ratio
$\bar{N}$ = injectant to freestream molecular weight ratio
p = static pressure
$\bar{p}$ = injectant to freestream static pressure ratio
p_0 = total pressure
Re = Reynolds number
$\bar{T}$ = injectant to freestream static temperature ratio
T_0 = stagnation temperature
U = velocity
$\bar{v}$ = injectant to freestream velocity ratio
w_i = width of nozzle exit plane
x = streamwise, axial coordinate
$\bar{x}$ = nondimensional distance downstream of the injection plane, x/h_i
y = cross-stream coordinate
$\bar{y}$ = nondimensional cross-stream coordinate, y/h_i
z = vertical coordinate
$\bar{z}$ = nondimensional vertical coordinate, z/h_i
$\bar{z}_j$ = jet liftoff height, helium mass flux center normalized by h_i
α_c = geometric compression angle of upper ramp surface
α_e = geometric expansion angle of channel between injector ramps
Γ = circulation
δ = boundary-layer height
$\bar{\delta}$ = nondimensional boundary layer-height, δ/h_i
$\bar{\rho}$ = injectant to freestream density ratio
ϕ = equivalence ratio
ω = vorticity vector

Received Nov. 21, 1991; revision received Sept. 16, 1992; accepted for publication Sept. 21, 1992.

*Assistant Professor, Department of Aeronautics and Astronautics. Member AIAA.
†Professor Emeritus, Mechanical Engineering Department. Fellow AIAA.
‡Professor, Mechanical Engineering Department. Fellow AIAA.

Introduction

THIS investigation was motivated by current efforts to develop a single-stage-to-orbit hypersonic vehicle. Through much of the flight envelope, the aircraft will be propelled by supersonic combustion ramjet (scramjet) engines relying on hydrogen-air reaction. For typical operating conditions, combustor flow speeds between 2000 and 5000 m/s will be realized, and the time-scale required for complete combustion of the oxidizer and fuel will be on the order of 1 ms. The problem of providing rapid molecular-scale mixing in this system is compounded by poor shear-induced mixing characteristic of high Mach number shear layers and by the requirement that a significant component of the momentum of the fuel be directed parallel to the intended thrust vector to derive as much thrust from the system as possible. Further, vehicle performance, in general, is closely tied to the efficacy of the combustion process.

The presence in scramjet combustors of both oblique shocks and strong fuel/air density gradients makes them an ideal arena for application of shock-enhanced mixing. The fuel injectors investigated in this study were aimed at enabling shock enhancement, and particular emphasis will be given to flow phenomena associated with this mixing mechanism.

Shock-Enhanced Mixing

Implementation of shock enhancement in a scramjet injection scheme was preceded by extensive efforts at the California Institute of Technology to study two-dimensional, unsteady shock interaction with circular gas inhomogeneities.[1-4] The predominant vorticity production mechanism associated with such an interaction is baroclinic torque. Consideration of the baroclinic source term in the vorticity equation

$$\rho \frac{\mathrm{D}}{\mathrm{D}t}\left(\frac{\omega}{\rho}\right) = \frac{1}{\rho^2} \nabla\rho \times \nabla p$$

shows that vorticity is generated in a fluid when pressure gradients and density gradients are nonparallel. For the two-dimensional case of shock passage over a circular region of light gas imbedded in air, imposition of the pressure gradient associated with the shock, on the density gradient at the interface between the air and the light gas, results in deposition of vorticity along the density gradient. The vorticity produces large-scale convective mixing and coalesces into a counter-rotating vortex pair. For a light gas inhomogeneity, the sense of the vortex pair is such that it migrates in the direction of shock motion.

Marble et al.[3] suggested this interaction as a canonical model for the case of the passage of a cylindrical jet of hydrogen fuel through an oblique shock wave. As the column of light gas passes through the pressure gradient associated with a weak oblique shock, streamwise vorticity will be deposited on the fuel/air interface. The vorticity will then act to modify the surface of the jet. Large-scale stirring of the flowfield will result directly in increased molecular-scale mixing as the interfacial area between the two gases is increased and species gradient dimensions are decreased. Further, Marble et al.[4] showed that the time scale in which the mixing occurs is short enough to be of interest for combustion enhancement in scramjet applications.

This work encouraged the exploration of a low drag injection system in which the basic concept of shock-generated streamwise vorticity could be incorporated into a scramjet combustor. A geometry was conceived in April 1987 and presented by Marble et al.[4] A diagram of the injection geometry is shown in Fig. 1. The injector consists of alternate compression ramps and expansion troughs. The end of each ramp houses a nozzle discharging the injectant. Fuel is injected parallel to the intended thrust vector to provide full utilization of the momentum of the injectant. In the plane of injection, the flow in the channels between the injectors is turned parallel to the freestream, forming a weak oblique shock. This shock is drawn on the side view of Fig. 1. The action of the shock is twofold. First, the pressure gradient associated with the shock intersects the density gradient existing between the light fuel and the air, generating axial vorticity. Second, based on the two-dimensional model, it was hypothesized that the vorticity would coalesce into a counter-rotating vortex pair of a sense that would cause migration of the fuel away from the wall. Thus, it was hoped that shock impingement would act to enhance both mixing and jet penetration.

Scope of the Investigation

The results presented here form the first part of a broad study of a class of contoured wall fuel injectors.[5] The goal of the study was to investigate the application of shock-enhanced mixing in a realistic scramjet injection geometry. The effort

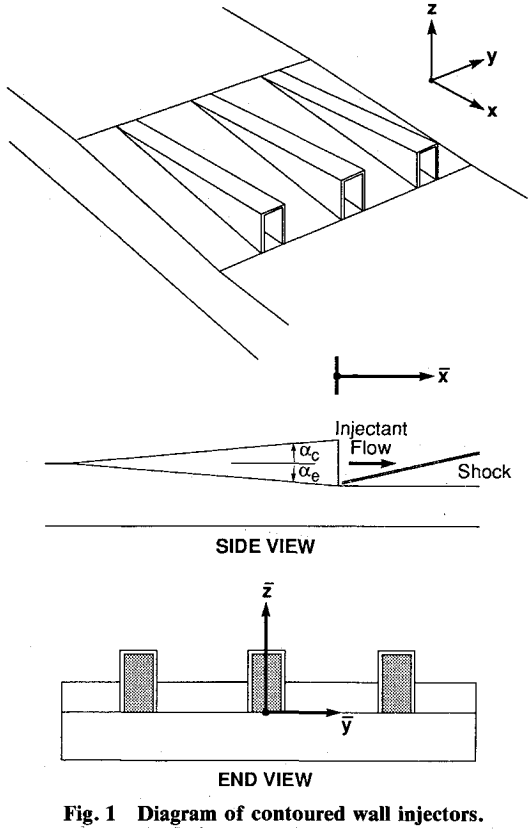

Fig. 1 Diagram of contoured wall injectors.

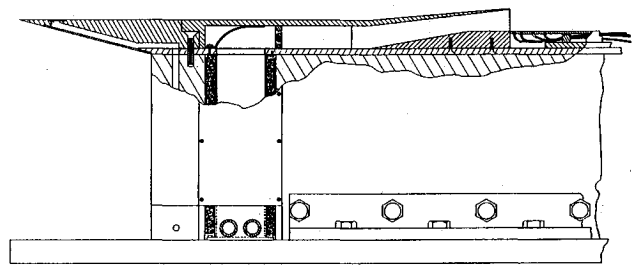

Fig. 2 Cross-sectional view of injector region of wind-tunnel model.

involved extensive experimental wind-tunnel testing as well as a significant computational effort to complement and extend the experimental investigations. The focus of this paper is the detailed description of flow phenomena associated with a single geometrical configuration subject to fixed injectant and freestream conditions.

The geometry was characterized by matched compression and expansion of the injector ramps ($\alpha_e = \alpha_c = 4.76$ deg) and array spacing such that the trough width was equal to approximately three times the width of the injection plane. The rectangular injector nozzles were 25.4-mm high, with an aspect ratio of 2 ($h_i = 2w_i$). Results from an array of three injectors are presented. Freestream conditions corresponded to $M = 6$, with helium injection at $M = 1.7$. Injectant conditions were chosen so that the injectant to freestream pressure and velocity ratios $\bar{p}$ and $\bar{v}$ were 1.0 and 1.33, respectively. The turbulent wall boundary layer entering the injectors was one-fifth the height of the injector ramps ($\bar{\delta} = 0.2$). Helium was used to simulate hydrogen fuel.

The applicability of the results of this study to scramjets is limited by two factors. The first of these is the inability to measure molecular-scale mixing. Unless otherwise stated, referrals to mixing performance relate to spatial and temporal scales, which were discernible within the experimental and computational resolution. The second limiting factor is the use of helium rather than hydrogen. Although the data presented give insight into the mixing-rate dominated combustion processes typical of scramjets, any dependence of fluid dynamics on chemical forcing will be absent.

The latter two parts of the broader effort are described in other publications[6,7] and were directed at 1) definition of salient parametric dependencies, including those associated with injector spacing, ramp geometry, wall boundary-layer effects, and injectant to freestream pressure and velocity ratios, and 2) characterization of the relative impact of various axial vorticity sources (including shock impingement) on circulation and mixing.

Experimental Apparatus and Methods

Experiments were conducted in the NASA Langley High Reynolds Number Mach 6 Wind Tunnel. The tunnel is an open-loop blowdown-type facility, with a 1-m long, 0.3-m-diam circular test section. The tests were conducted at $p_0 = 6.9$ MPa, $T_0 = 520$ K, with a freestream Reynolds number of 5×10^6/m. A modular wind-tunnel model was designed to allow testing of a variety of injector configurations. A cross-section view of the injector region of the model is shown in Fig. 2. The injector geometry discussed in this paper was identical to that of Fig. 1, with three injectors spanning the upper plate laterally. Helium was injected horizontally through two-dimensional, $M = 1.7$ nozzles. Four rake-mounted probes were used to investigate the flow: a cone static pressure probe, a pitot probe, a total temperature probe, and a composition probe.

Helium Concentration Measurements

The composition probe was based on the response of a hot-film anemometer sensor in a binary gas mixture. The

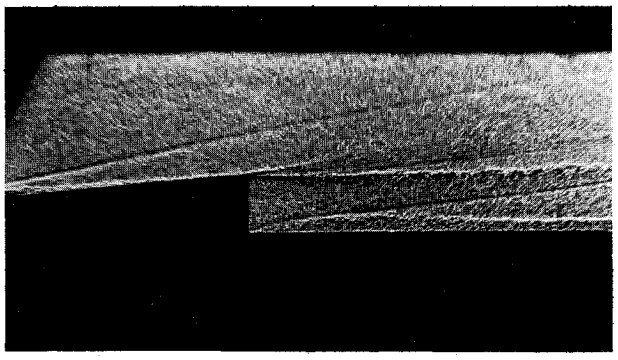

Fig. 3 Shadowgraph of injector flowfield.

design and application of this device are presented in detail in Ref. 5. In a helium-air gas mixture, the anemometer output E is a function of pressure, temperature, velocity, and composition. A sample was withdrawn from the flowfield and allowed to pass over a hot-film sensor. The sensor was located upstream of a choked orifice such that velocity was fixed for a given pressure, temperature, and composition. Further, prior to passage over the hot film, the gas sample was thermally fixed by using a heat exchanger and, in fact, locating the entire device within an ice-water bath. While removing an additional variable from the problem, thermal conditioning also enhanced sensitivity, effectively increasing the allowable overheat ratio for the hot-film anemometer. (Without cooling the sample, the high total temperatures in the flow would have allowed only very slight overheat without exceeding the operating temperature for the hot film.) Thus, the velocity and temperature were fixed for a given pressure and composition, and E was dependent only on pressure and helium mass fraction. Pressure was measured at the location of the hot-film sensor. An automated calibration system was developed that allowed daily calibration of device response to pressure and composition. In practice, a sample was withdrawn from the flow, the pressure at the hot-film location p and the anemometer output were measured, and composition was determined from a bilinear interpolation of E and p in the calibration space.

A quartz-coated hot-film sensor was used rather than a hot-wire sensor because of the calibration drift that results from changes in the thermal accommodation coefficient for hot-wire probes in helium-air mixtures.[8,9] Care was taken to assure that sufficient mass flow was sustained through the probe so that the bow shock that formed ahead of the sampling tip was swallowed. The sampling tip was designed with an internal expansion to make this possible. If the shock is not swallowed, the strong pressure gradients existing between the shock and the probe tip cause preferential deflection of light gas species around the probe so that the sample is enriched with heavy gas species. Separation of gas species in this manner can be nearly complete,[10-12] and proper design and mass flow monitoring are imperative for accurate sampling.

In final form, the gas sampling apparatus allowed determination of helium mole fraction with less than $\pm 3\%$ error throughout the entire operating envelope ($M = 6$ air at $p_0 = 6.9$ MPa, $T_0 = 520$ K, to $M = 1.7$ helium at $p_0 = 0.023$ MPa, $T_0 = 220$ K). Response time on the order of 1.5 s, combined with wind-tunnel run times of greater than 1 h, allowed detailed surveying of the injector flowfield.

Flow Visualization

A collaborative effort was undertaken with personnel from the Optical Spectroscopy Section of the NASA Langley Research Center, Instrument Research Division, to investigate the application of planar Rayleigh scattering in the High Reynolds Number Mach 6 Wind Tunnel. All issues associated with the application of this technique as a diagnostic measure were resolved by NASA personnel (particularly Shirinzadeh, Balla, Hillard, Anders, and Exton). Difficult conditions in the wind tunnel precluded use of the technique as a quantitative tool. In fact, even qualitative evaluations were hindered by various complicating factors, including molecular clustering and possible solidification of some species. The technique provided temporally resolved planar images that, in light of comparisons with the time-mean flow survey data, allowed insight into the flow that was vital in estimating the scale and importance of unsteady phenomena. A detailed presentation of the apparatus, sampling procedures, postprocessing methods, and limiting factors has been presented by Shirinzadeh et al.[13] Discussions of the influence of molecular clustering on Rayleigh measurements in a similar flowfield are contained in Refs. 14 and 15.

Computational Methodology

The difficulties associated with the experimental investigation of the contoured wall fuel injectors made application of numerical modeling an attractive complement to the experimental effort. For these purposes the SPARK3D code[16] was obtained from the Computational Methods Branch at NASA Langley Research Center. The program integrates the three-dimensional Navier-Stokes, energy, and species continuity equations for a multiple species system undergoing chemical reaction. It has been used by several investigators to predict reacting and nonreacting flow about other scramjet injector geometries.[16-19] For this study, the code was used in a nonreacting mode with $M = 1.7$ helium injected into $M = 6$ air to allow direct comparison with the experiments. The system of equations was advanced in time until convergence at steady state was obtained. Typical domains consisted of 266,000 grid points. First-order boundary conditions were applied to simulate an infinite array of injectors. Viscous conditions were applied on the walls of the injector. Open boundary treatment was used on the top of the domain. The difficulty in accurately representing complex turbulent mixing phenomena prompted a decision to limit the scope of the computations to laminar simulations. Thus, mixing rates were not captured accurately. Pressure, temperature, and large-scale ($> 1/5h_i$) flow structure were reproduced.

Results

An introduction to flow phenomena about the injectors is provided by consideration of the temporally resolved (30 ns pulse duration) shadowgraph of the flowfield shown in Fig. 3. Flow is left to right. Both the shock generated by the beginning of the injector ramps and that due to turning of the flow between the ramps at the exit plane are apparent. The latter of these was responsible for baroclinic vorticity generation through interaction with the density gradients associated with the injectant/air interfaces. Passage of the helium jet (represented by the two parallel white lines that intersect the right edge of the photograph nearly perpendicularly) between the shocks formed from turning of the flow in the troughs is evidence that the contoured wall geometry provided shock impingement as envisioned. Note the extent of the separation between the lower boundary of the jet and the wall.

The shock generated by the compression of the upper ramp surface foretells additional axial vorticity generation mechanisms associated with the ramps. High pressure existed above the ramps, with lower pressure fluid in between. The pressure imbalance generated flow from the upper surface of the ramps, producing 1) strong axial vorticity through turning of the cross-stream vortex lines associated with the boundary layer, and 2) additional diffusion of vorticity along the ramp sidewalls. These mechanisms were the source of local cross-stream shear between the injectant and the airflow.

Flowfield Survey

The dynamics of the helium jet are displayed in more detail in Fig. 4. Contours of constant helium mass fraction are shown for various axial stations downstream of the injection plane ($\bar{x} = 0$, 1, 4, 8, and 13). The data were obtained using the

composition probe previously described and have been mirrored about the plane of symmetry at $\bar{y} = 0$. The edges of each of the plots correspond to the planes of symmetry between the injectors in the array. The maximum helium mass fraction is tabulated above each of the plots. It must be emphasized that these data are time mean, and the manifestation of the unsteady component of the flow in these plots has not been addressed. Also, in these plots and others shown, subgrid-scale features should not be interpreted. The experimental sampling grid has been overlaid on one of the plots of Fig. 4.

The strong liftoff of the jet apparent in the shadowgraph is clear in these data as well. Complete separation of the jet from the surface occurred at approximately one injector height downstream of injection. The formation of a counter-rotating vortex pair in the helium jet is evidenced by the form of the helium signatures. The sense of the vorticity was such that the pair migrated from the wall into the freestream.

More details of the flow about the ramps are displayed in the pitot pressure surveys shown in Fig. 5. High pressure existed above the ramps from the compression of the upper ramp surface, and low pressure existed between, due to expansion in the troughs. This pressure gradient drew the boundary layer from the compression surfaces and into the troughs between the ramps, and it was fundamental in producing shear between the injectant and the air along the ramp trailing edge. Displacement associated with the hypersonic boundary layer modified the effective wall geometry from the perspective of the flow external to the boundary layer. Consideration of the pitot pressure contours in the injection plane, however, shows that the boundary layer did not inhibit shock formation in the vicinity of the helium/air density gradients. Counter to expectations, a tongue of high-momentum flow was maintained in the corner of the troughs, with the low-momentum boundary-layer fluid collecting in the center of the passageway. This allowed shock formation precisely where it was required to produce baroclinic torque: the region of helium/air density gradients. (The interaction with the boundary layer was not benign, however, for some of the other injector spacings and boundary-layer thicknesses tested.[6])

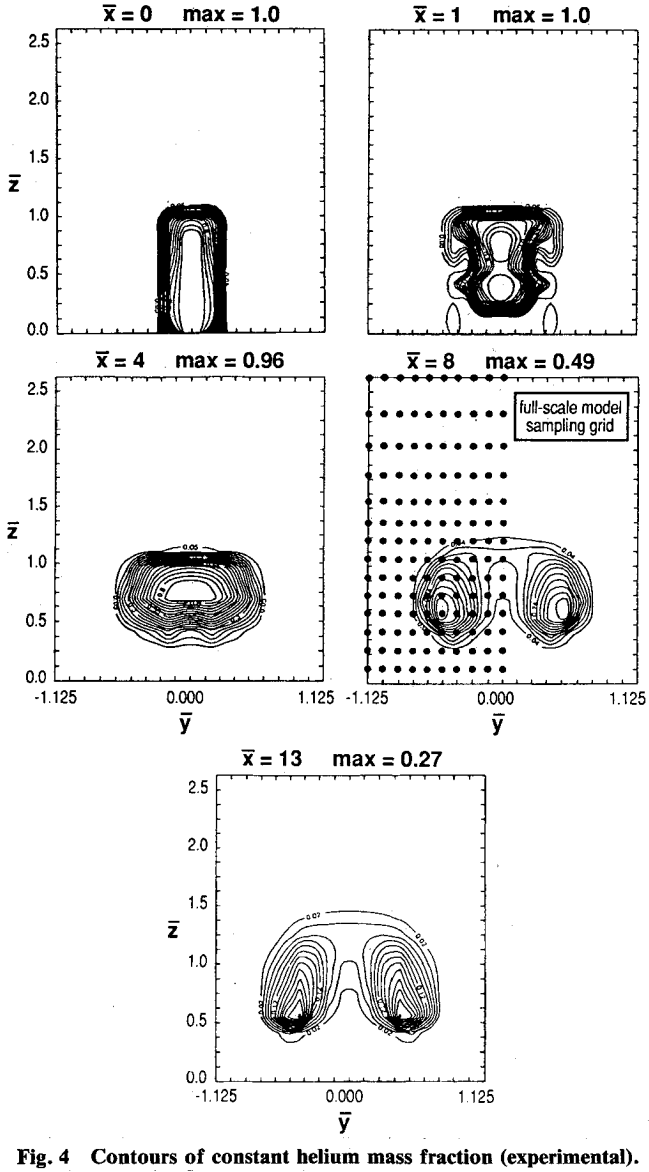

Fig. 4 Contours of constant helium mass fraction (experimental).

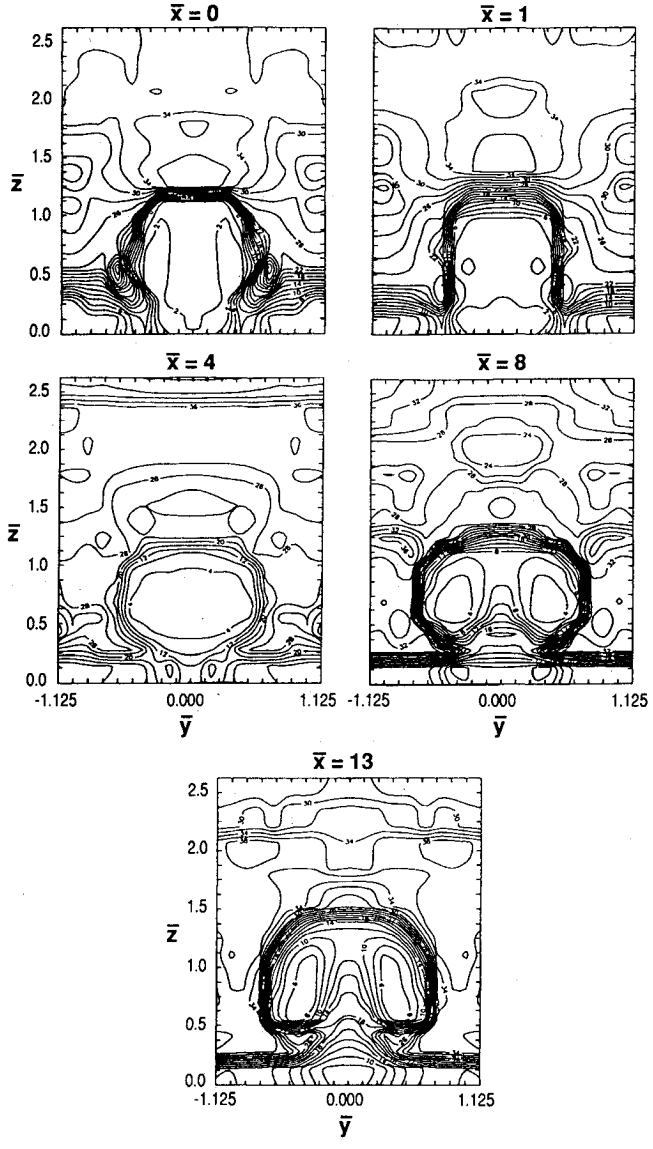

Fig. 5 Contours of constant pitot pressure (experimental).

Numerical Simulation

For comparison purposes the numerical data have been plotted in the same form, scale, and axial locations as the experimental data. Helium mass fraction and pitot pressure are shown in Figs. 6 and 7. The spacing between the injectors for the computational case was slightly different from that of the experimental case, and the plots extend to $\bar{y} \pm 1.0$ rather than $\bar{y} \pm 1.125$. The spatial resolution provided by the computational grid was considerably better than that of the experiments. The grid has been overlaid on one of the plots of Fig. 6. Since no attempt was made to model the turbulent mixing phenomena accurately, the mass fraction levels displayed in the simulation differ from those measured experimentally.

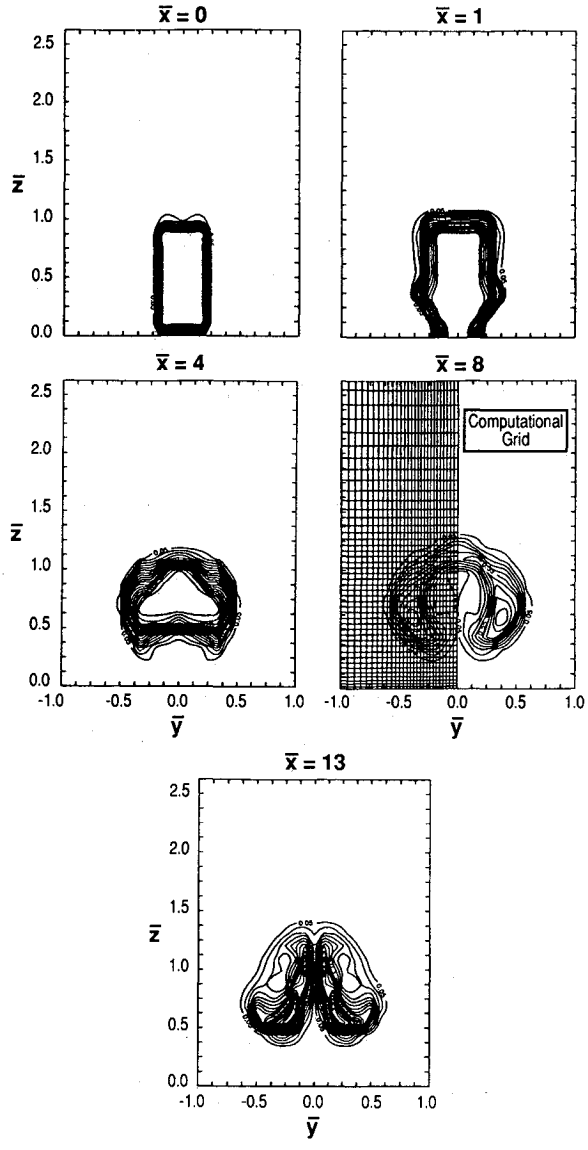

Fig. 6 Contours of constant helium mass fraction (computational).

However, the qualitative behavior and the location and form of the species gradients were accurately captured by the computations. Close qualitative and quantitative agreement was found between the experimentally and numerically obtained pitot pressure contours (Figs. 5 and 7, respectively). The level of agreement between the experiments and the simulation was sufficient to allow the numerical data to be used in parallel with the experimental data to describe many flow features.

Figure 8 contains a perspective view of data obtained from the numerical simulation showing the behavior of the helium jet farther downstream from the nozzle. The helium signatures produced by jet interaction with the counter-rotating vortex pair are reminiscent of those seen for the canonical problem of two-dimensional, unsteady shock impingement on a circular light gas inhomogeneity.[1-4] The analogy between this and the current problem is limited, however, by other significant sources for vorticity in the flowfield (primarily variation in aerodynamic loading on the ramp surfaces) and three-dimensional effects.

Subgrid Scale Structure

Having presented the numerical and experimental contour plots, it is appropriate to discuss how accurately they represent the flow. The influence of limited spatial resolution on the form of the time-mean helium signatures is considered first. The effects of unsteadiness are addressed in the following section.

Considering the relative injectant transport due to diffusion and convection in the steady (and laminar) numerical simulation, it is apparent that the detailed form of the helium jet was not accurately captured. A qualitative demonstration of the level of convective mixing associated with the axial vorticity is provided by considering the particle traces from neighboring points in the flowfield shown in Fig. 9. The particle path marked with the solid line makes three complete orbits about the vortex core by $\bar{x} = 30$. Notably, the two helium particles, located one just above the other, take considerably different paths through the domain, with the lower particle exhibiting an additional orbit. Fluid interfaces are stretched, and injectant/freestream gradient dimensions are narrowed.

This strong convection can then be compared to the rate of growth of helium/air diffusion gradients. The average depth of penetration of a molecule in a species gradient was approximated to be only 3.3% of h_i by the end of the computational domain. This suggests that much of the mixing region, if sufficiently resolved, would appear in the form of tightly rolled, spiral species gradients not yet merged due to diffusion. (In fact, recent experimental data presented by Budzinski[20] support this hypothesis.) This signature would be hidden by artificial viscosity and spatial discretization in the computations and by the spatial averaging of the probes,

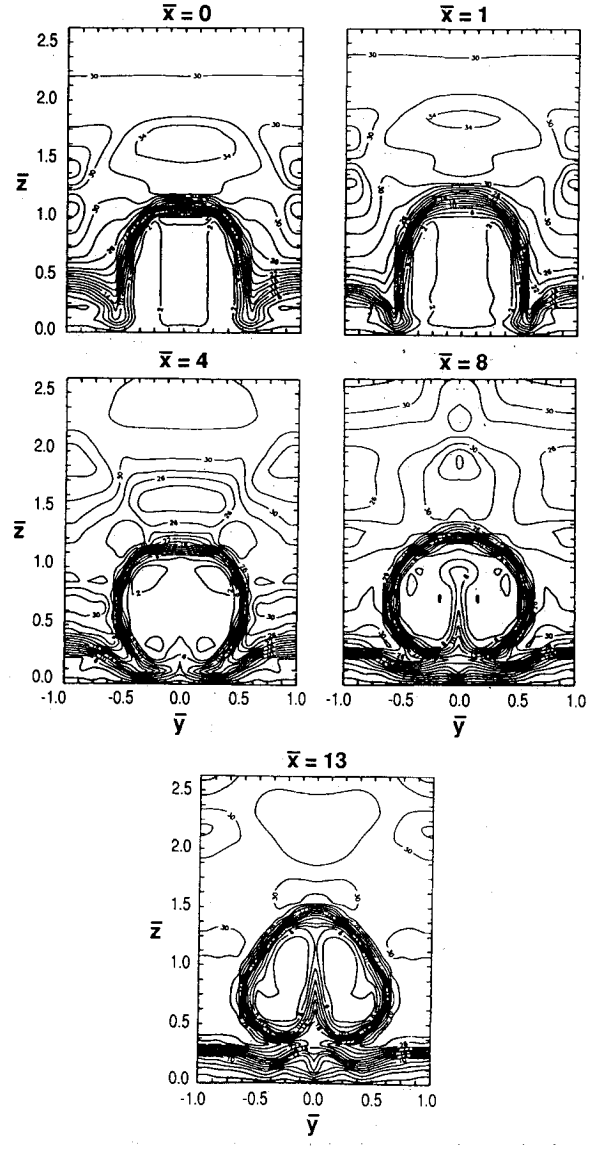

Fig. 7 Contours of constant pitot pressure (computational).

limited spatial resolution of the sampling grid, and unsteadiness in the experiments.

Time-Fluctuating Flow

Temporally resolved (15 ns pulse duration), planar Rayleigh scattering was employed to impart a qualitative knowledge of the level and importance of the time-fluctuating component of the flowfield. Prior to presenting the time-resolved data, the limitations of the imaging technique will be addressed through a comparison with the time-mean, rake survey data.

Four plots are shown in Fig. 10. Figure 10b is an average of 22 instantaneous, planar Rayleigh images taken at $\bar{x} = 10$. Included in the figure are contour plots of experimental static pressure, static temperature (both obtained from the raw data through the reduction technique described in Ref. 5), and helium mass fraction data. (Because of limitations associated with molecular clustering, the optical technique was applied at $T_0 = 520$ K, $p_0 = 4.1$ MPa, resulting in a Reynolds number of 3×10^6/m. Whereas the other tests presented were conducted at $Re = 5 \times 10^6$/m, the rake survey data shown in Fig. 10 were obtained at $Re = 3.5 \times 10^6$/m: $T_0 = 520$ K and $p_0 = 4.8$ MPa, to allow closer comparison with the Rayleigh data.) The data are scaled linearly between zero and the maximum signal level in the image. Some regions of the flowfield (e.g., the core of the helium jet and the base of the boundary layer) were below the sensing threshold of the instrumentation. White bands have been added to the gray scale to aid in identification of intensity gradients in the images. The dynamic range and spatial resolution of the Rayleigh measurements did not allow analysis of the fine-scale structure within the jet.

Since the scattering cross section for helium is much less than that for the air, lower signal levels are expected in regions containing significant concentrations of helium. Cursory analysis of these plots, however, shows that to first-order variations in intensity in the Rayleigh images correspond to variations in

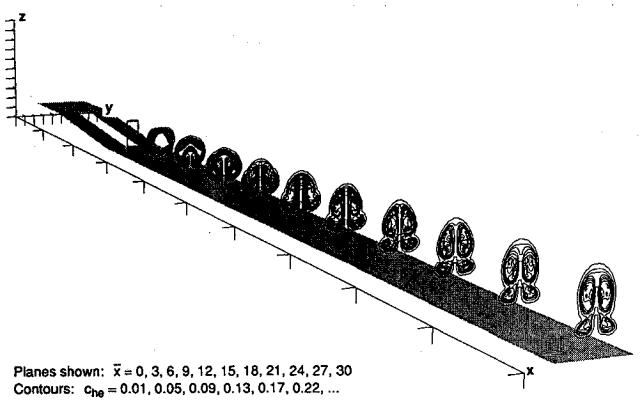

Fig. 8 Perspective view of jet development. Contours of constant helium mass fraction (computational).

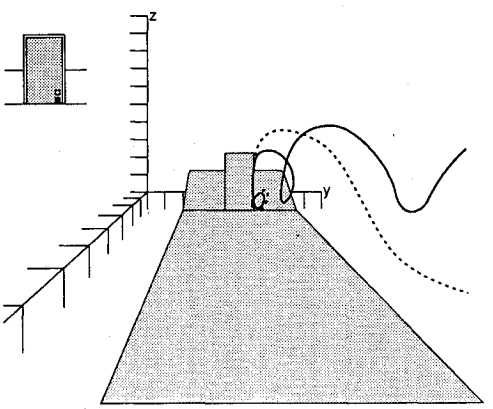

Fig. 9 Particle traces.

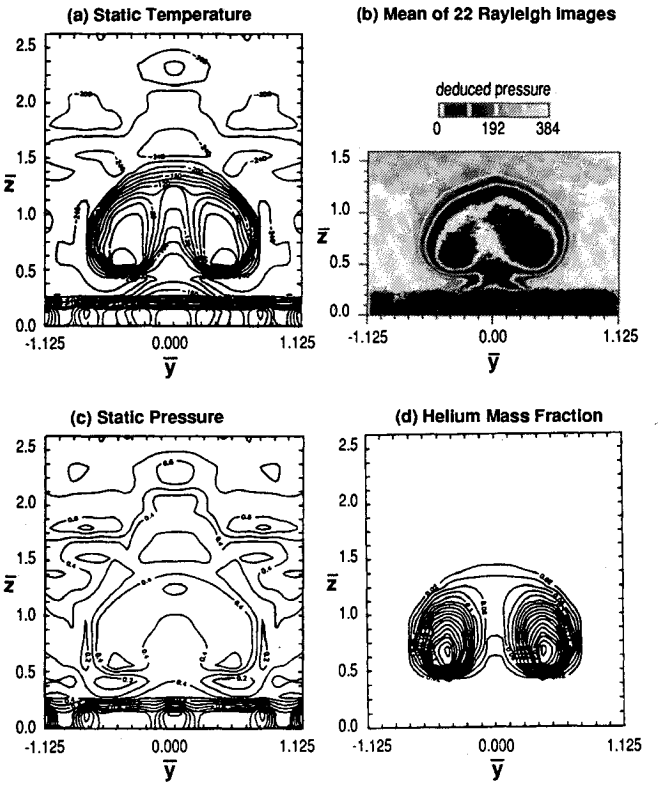

Fig. 10 Comparison of experimental mean survey data with mean of 22 planar Rayleigh images at $\bar{x} = 10$.

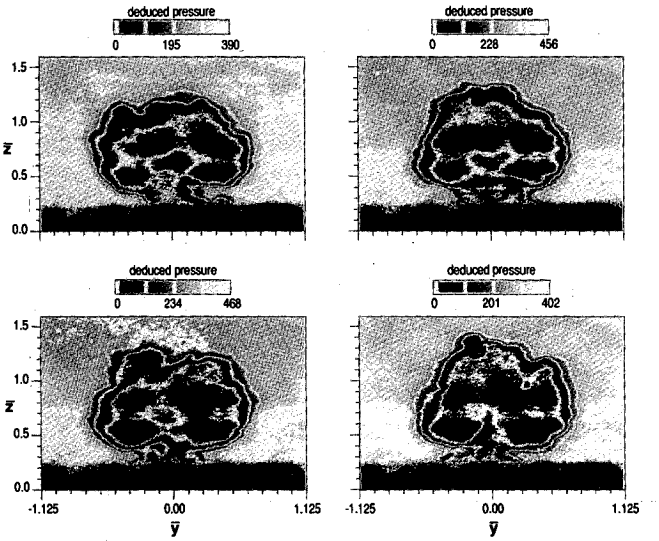

Fig. 11 Instantaneous planar Rayleigh images at $\bar{x} = 10$.

static temperature in the flowfield rather than helium concentration. This is due in part to the strong dependence of molecular clustering on local temperature. Thus, the representation of the location of gradients in helium mass fraction is accurate only in regions where the species gradients were coincident with pressure or temperature gradients, and the utility of the method for tracking the mixing interface is strongly limited.

These limitations must be considered in interpreting the samples of time-resolved data that are presented in Fig. 11. On the sides and top edges of the jet, it is assumed that lines of constant image intensity correspond to lines of roughly constant helium mass fraction. Below the jet, a similar conclusion is not allowed, as pressure and temperature gradients were not coincident with species gradients as previously described. In particular, gas sampling measurements show that the stem that appears below the jet did not contain any helium (see Fig.

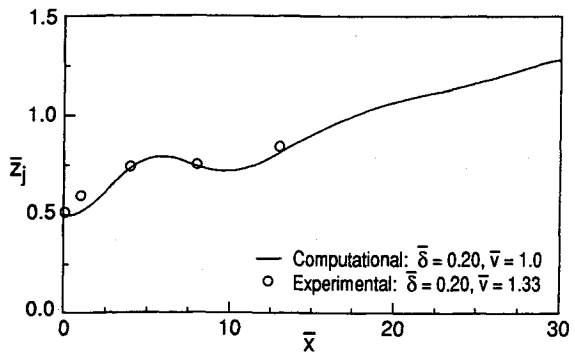

Fig. 12 Liftoff height of helium jet from surface.

10d). It was merely warmer, lower pressure air entrained in part from the boundary layer. (The boundary layer appears as a dark band stretching across the bottom of each of the images.) The maximum peak-to-peak spatial amplitude of the unsteady oscillations of the intensity gradients about the mean in these images is approximately $0.4h_i$.

These data, along with images from an axial location further upstream, were used to estimate the extent to which mixing was dominated by unsteady effects. The scale of the unsteadiness in the Rayleigh images suggests that for $\bar{x}>5$, turbulence became progressively more important. Certainly, the strong large-scale convection displayed in the particle traces of Fig. 9 and the turbulent mixing were superposed. The measurements were not sufficiently resolved to determine whether this superposition acted to damp turbulent mixing, but studies of other vortical mixers[21] suggest that the interaction is positive in terms of the overall molecular mixedness of the flowfield. The level of unsteadiness displayed in the images also suggests that turbulent mixing would disrupt any far-field species stratification that might occur due to the pressure gradients associated with the vortical motion.

Analysis of Performance

The liftoff height of the jet from the surface $\bar{z}_j$ is compared for the experimental and numerical data in Fig. 12. This was calculated from the numerical data as the helium mass flux center and was approximated using the experimental data by calculating the helium mass fraction center. The agreement between the experimental data and the simulation is excellent. The dip in the curve is a result of the dynamics of the helium as it was acted upon by the vorticity field. After coalescing into a counter-rotating vortex pair, migration from the wall at a constant slope of $\bar{z}_j/\bar{x} = 0.025$ occurred. By $\bar{x} = 30$, the mass flux center was located at $\bar{z} = 1.3$, with the point of maximum penetration at $\bar{z} = 2.0$. Possibly more important than the bulk behavior of the jet for heating considerations was the complete liftoff of the jet from the surface. Impingement upon the injectant/air density gradients with a shock that was generated at the base of the jets was identified as the factor that provided complete liftoff.[5] Notably, impingement upon the jets from above, such as with a reflected shock, acts to produce vorticity of an opposite sense. If this vorticity is dominant, a counter-rotating vortex pair will be formed of a sense that will cause an undesirable migration of the jet toward the wall.

The circulation present in each y-z computational plane is plotted in Fig. 13. Careful interpretation is required since the value of circulation in all regions was strongly influenced by distortion of the vortex lines associated with the boundary layer. The observations presented below resulted from studying the vorticity field using three-dimensional flow visualization software. The growth in circulation that begins at $\bar{x} = -6.0$ (which corresponds to the start of the ramps) is one portion of what might loosely be termed "ramp-generated vorticity," and it resulted from turning of the incoming vortex lines associated with the boundary layer and further diffusive vorticity flux from the ramp walls. These sources were fundamental in producing cross-stream shear between the air and the injectant at the nozzle exit. At $\bar{x} = 0$, a large increase in circulation occurred. This resulted from 1) vorticity production from baroclinic torque due to shock impingement on injectant/air density gradients, and 2) further turning of the boundary flow. Thus, although it was apparent that axial vorticity was produced by shock impingement, it was also clear that other vorticity sources of similar magnitude were present in the flowfield. It is important to note, however, that the utility of shock enhancement is not only the additional streamwise vorticity produced, but also the location of that vorticity with respect to the fuel/air interface. Baroclinic torque provides for deposition of vorticity directly on the fuel/air interface.

The experimental peak injectant mass fraction levels in each measurement plane are plotted in Fig. 14. Data from a half-scale model test have been included to show the behavior at larger nondimensional distances from the injection plane. Although not a satisfying measure of molecular mixing, this time-averaged measure of performance is frequently used as a means for comparison because of the relative ease with which it may be obtained. A maximum decay slope of 12% mass fraction per injector height downstream occurred between $\bar{x} = 5$ and $\bar{x} = 10$. For $\bar{x} \geq 4$ the decay was fit with a power law proportional to $\bar{x}^{-1.37}$.

It is important to cast the jet penetration and mixing performance previously described in light of pertinent fuel/air mass flux ratios for scramjet applications. This was done by considering the freestream area required relative to the area of the nozzle exit plane, if the fuel were to be homogeneously mixed to a desired mass fraction for a given set of conditions. Such considerations can yield an estimate for the combustor length required for a given injector geometry.

The area ratio required to provide a desired equivalence ratio ϕ for a given set of injectant and freestream conditions may be expressed as

$$\bar{A} = \frac{\phi \bar{m}_{st} \bar{T}}{\bar{p} \bar{N} \bar{v}}$$

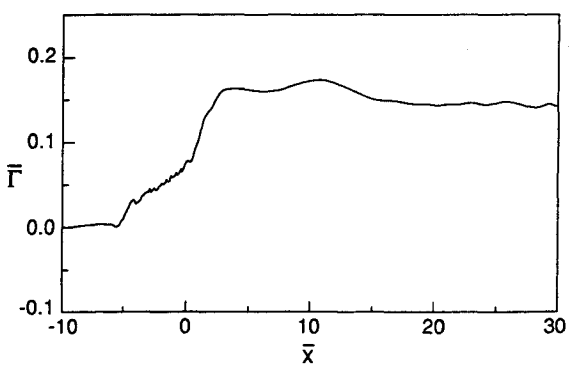

Fig. 13 Circulation nondimensionalized by $U_\infty h_i$ in the y-z plane (computational).

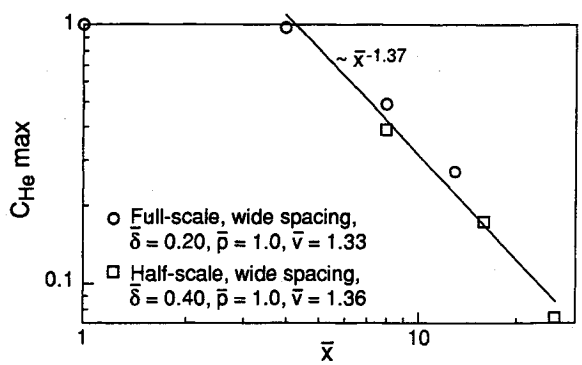

Fig. 14 Peak helium mass fraction decay (experimental).

where the subscript "st" refers to stoichiometric. For typical scramjet operating conditions ($\phi = 1.0$, $\bar{m}_{st} = 0.03$, $\bar{N} = 2/29$, $\bar{p} = 1.0$, $\bar{v} = 1.0$, and $\bar{T} = 1/6$), $\bar{A} = 0.07$. The injectant must be mixed into an area approximately 15 times the area of the injector nozzle. (For the specific conditions of this study with $\phi = 1.0$, $\bar{m}_{st} = 0.03$, $\bar{N} = 4/29$, $\bar{p} = 1.0$, $\bar{v} = 1.33$, and $\bar{T} = 2.5$, the area ratio is much higher, with $\bar{A} = 0.41$. The high static temperature ratio is only partially offset by the increased molecular weight of the injectant. Considerably less air would be required to be entrained by the helium jet.) If this area is fixed laterally by the planes of symmetry separating each of the jets in the array, then the vertical extent of the area would be approximately $\bar{z} = 4.0$ for this injector spacing. For the freestream velocities of these tests, penetration on that order would be expected by $\bar{x} \approx 60$. This, then, is an estimate for the minimum required combustor length. The estimate is conveniently devoid of dependence on detailed mixing rate data, based instead on kinematical aspects of the flow that are predicted with better accuracy, both computationally and experimentally. Additional combustor length would be required if mixing augmentation, diffusion, and turbulent processes have not produced uniform, molecularly mixed fluid by this point.

Conclusions

An investigation of a contoured wall fuel injector has been presented. The injector was designed to enable shock-enhanced mixing for scramjet combustor applications. Shock impingement was one of several vorticity sources identified in the flowfield. Further work continues to quantify the relative impact of these sources on circulation and mixing.[7] The vorticity field coalesced into a counter-rotating vortex pair of a sense that caused the helium jet to migrate away from the surface. A constant jet trajectory slope of 0.025 was found for $\bar{x} > 20$. Further, an increase in interfacial surface area and narrowing of species gradients were afforded by the strong convective forces. Estimation of convective and diffusive phenomena showed that, in the near field, the internal structure of the jet may take the form of tightly wound, spiral species gradients. Farther downstream this structure would be disrupted by turbulent processes. Temporally resolved planar Rayleigh imaging was used to provide qualitative insight into the scale and nature of the time-fluctuating flow component. The peak-to-peak spatial amplitude of the unsteady oscillations of image intensity about the mean was as large as 4/10 of the injector height at $\bar{x} = 10$.

Experimentally, the peak helium mass fraction decay was proportional to $\bar{x}_j^{-1.37}$. For representative scramjet combustor conditions, it was projected that complete mixing of the hydrogen fuel to less than the stoichiometric mass fraction would require jet penetration into an area approximately 15 times the area of the injection plane. For the freestream velocities of this study, such behavior would be expected by $\bar{x} \approx 60$.

Several salient parametric dependencies have been investigated for the contoured wall fuel injectors. The parameters investigated include injector spacing, combustor wall boundary-layer height, and injectant to freestream pressure and velocity ratios. These are discussed in another publication.[6]

Acknowledgments

Funding for this work was provided largely through NASA Grant NAG1-842. The authors wish to thank many members of the technical staff at NASA Langley Research Center, particularly D. Bushnell, members of the Experimental Flow Physics Branch, and members of the Computational Methods Branch. The Rayleigh scattering data were obtained through a collaborative effort with B. Shirinzadeh, J. Balla, M. Hillard, and R. Exton of the Instrument Research Division's Optical Spectroscopy Section. Supercomputing support was provided by the San Diego Supercomputer Center via a National Science Foundation grant, the NASA Ames Numerical Aerodynamic Simulation facility, the Jet Propulsion Laboratory/Caltech Cray, and the NASA Langley supercomputing facilities.

References

[1]Haas, F., and Sturtevant, B., "Interaction of Weak Shock Waves with Cylindrical and Spherical Gas Inhomogeneities," *Journal of Fluid Mechanics,* Vol. 181, Aug. 1987, pp. 41–76.

[2]Yang, J., "An Analytical and Computational Investigation of Shock-Induced Vortical Flows with Applications to Supersonic Combustion," AIAA Paper 92-0316, Jan. 1992.

[3]Marble, F. E., Hendricks, G. J., and Zukoski, E. E., "Progress Toward Shock Enhancement of Supersonic Combustion Processes," AIAA Paper 87-1880, July 1987.

[4]Marble, F. E., Zukoski, E. E., Jacobs, J. W., Hendricks, G. J., and Waitz, I. A., "Shock Enhancement and Control of Hypersonic Mixing and Combustion," AIAA Paper 90-1981, July 1990.

[5]Waitz, I. A., "An Investigation of Contoured Wall Injectors for Hypervelocity Mixing Augmentation," Ph.D. Dissertation, California Inst. of Technology, Pasadena, CA, 1991.

[6]Waitz, I. A., Marble, F. E., and Zukoski, E. E., "A Systematic Experimental and Computational Investigation of a Class of Contoured Wall Fuel Injectors," AIAA Paper 92-0625, Jan. 1992.

[7]Waitz, I. A., Marble, F. E., and Zukoski, E. E., "Vorticity Generation by Contoured Wall Fuel Injectors," AIAA Paper 92-3550, July 1992.

[8]Mcquaid, J., and Wright, W., "The Response of a Hot-Wire Anemometer in Flows of Gas Mixtures," *International Journal of Heat and Mass Transfer,* Vol. 16, No. 4, 1973, pp. 819–828.

[9]Simpson, F. L., and Wyatt, W. G., "The Behavior of Hot-Film Anemometers in Gas Mixtures," *Journal of Physics E: Scientific Instruments,* Vol. 6, No. 10, 1973, pp. 968–1060.

[10]Reis, V. H., and Fenn, J. B., "Separation of Gas Mixtures in Supersonic Jets," *Journal of Chemical Physics,* Vol. 39, No. 12, 1963.

[11]Chang, J. H., and Fenn, J. B., "Species Separation by Stagnation of Argon-Helium Mixtures in Supersonic Flow," *Proceedings of the Seventh Rarefied Gas Dynamics Symposium,* Editrice Tecnico Scientifica, Pisa, Italy, 1970, pp. 599–607.

[12]Campargue, R., "The Separation Probe," *Aerodynamic Separation of Gases and Isotopes,* Lecture Ser. 82, von Kármán Inst. for Fluid Dynamics, Rhode Saint Genese, Belgium, Jan. 5–9, 1976.

[13]Shirinzadeh, B., Waitz, I. A., Balla, J., Hillard, M. E., Anders, J. B., and Exton, R. J., "Planar Rayleigh Scattering Results in Helium/Air Mixing Experiments in a Mach 6 Wind Tunnel," *Applied Optics,* Vol. 31, No. 30, Oct. 1992.

[14]Shirinzadeh, B., Hillard, M. E., and Exton, R. J., "Condensation Effects on Rayleigh Scattering Measurements in a Supersonic Wind Tunnel," *AIAA Journal,* Vol. 29, No. 2, 1991, pp. 242–246.

[15]Shirinzadeh, B., Hillard, M. E., Blair, A. B., and Exton, R. J., "Study of Cluster Formation and Its Effects on Rayleigh and Raman Scattering Measurements in a Mach 6 Wind Tunnel," AIAA Paper 91-1496, June 1991.

[16]Carpenter, M. H., "Three-Dimensional Computations of Cross-Flow Injection and Combustion in a Supersonic Flow," AIAA Paper 89-1870, June 1989.

[17]Drummond, J. P., Carpenter, M. H., Riggins, D. W., and Adams, M. S., "Mixing Enhancement in a Supersonic Combustor," AIAA Paper 89-2794, July 1989.

[18]Eklund, D. R., Northam, G. B., and Fletcher, D. G., "A Validation Study of the SPARK Navier-Stokes Code for Nonreacting Scramjet Combustor Flowfields," AIAA Paper 90-2360, July 1990.

[19]Riggins, D. W., Mekkes, G. L., McClinton, C. R., and Drummond, J. P., "A Numerical Study of Mixing Enhancement in a Supersonic Combustor," AIAA Paper 90-0203, Jan. 1990.

[20]Budzinski, J. M., "Planar Rayleigh Scattering Measurements of Shock Enhanced Mixing," Ph.D. Dissertation, California Inst. of Technology, Pasadena, CA, 1992.

[21]Elliot, J. K., Manning, T. A., Qui, Y. J., Greitzer, E. M., Tan, C. S., and Tillman, T. G., "Computational and Experimental Studies of Flow in Multi-Lobed Forced Mixers," AIAA Paper 92-3568, July 1992.